

Mesh distortion sensitivity of 8-node plane elasticity elements based on parametric, metric, parametric-metric, and metric-parametric formulations

S. Rajendran[†]

*School of Mechanical and Production Engineering, Nanyang Technological University,
Nanyang Avenue, Singapore 639798*

S. Subramanian[‡]

Microwave Tube Research and Development Centre, Jalahalli, Bangalore 560013 India

(Received July 16, 2003, Accepted December 2, 2003)

Abstract. The classical 8-node isoparametric serendipity element uses parametric shape functions for both test and trial functions. Although this element performs well in general, it yields poor results under severe mesh distortions. The distortion sensitivity is caused by the lack of continuity and/or completeness of shape functions used for test and trial functions. A recent element using parametric and metric shape functions for constructing the test and trial functions exhibits distortion immunity. This paper discusses the choice of parametric or metric shape functions as the basis for test and/or trial functions, satisfaction of continuity and completeness requirements, and their connection to distortion sensitivity. Also, the performances of four types of elements, viz., parametric, metric, parametric-metric, and metric-parametric, are compared for distorted meshes, and their merits and demerits are discussed.

Key words: eight-node plane element; parametric-metric element; unsymmetric finite element; mesh distortion; geometric distortion; higher order completeness.

1. Introduction

The classical 8-node serendipity isoparametric quadrilateral element is a widely used element for plane stress/strain applications. This element uses parametric shape functions that involve a complete quadratic polynomial ξ and η with the addition of two cubic terms, $\xi^2\eta$ and $\xi\eta^2$ (e.g., see Zienkiewicz and Taylor 1989). The 9-node Lagrangian isoparametric quadrilateral element is also widely used for plane stress/strain applications. This element also uses parametric shape functions that involve a complete quadratic polynomials in the natural coordinates, ξ and η , but with three additional terms, $\xi^2\eta$, $\xi\eta^2$, and $\xi^2\eta^2$ (e.g., see Zienkiewicz and Taylor 1989). The performance of 9-node Lagrangian isoparametric element is very similar to that of 8-node serendipity isoparametric

[†] Assistant Professor

[‡] Scientist

element for meshes involving square and rectangular element geometry. For such meshes, the 8-node element is often preferred to the 9-node element because the later uses an extra node at the centre of the element. However, the performance of 9-node element is better than that of 8-node element under some types of mesh distortion (Lee and Bathe 1993). Lee and Bathe (1993) showed that the 8-node element can at best reproduce exactly a linear polynomial displacement field (in global Cartesian coordinates) under the angular distortion as well as quadratic curved-edge distortion. On the other hand, the 9-node element can reproduce exactly a quadratic displacement field under angular distortion, and a linear field under quadratic curved-edge distortion. However, a full (3×3) numerical integration of stiffness matrix needs to be employed for 9-node element, whereas, for the 8-node isoparametric element, a reduced order (2×2) numerical integration generally produces accurate solution under distorted mesh. With the reduced order integration, the performance of the 9-node element is, however, worse than that of the 8-node element. An excellent comparison of these two elements is given by MacNeal and Harder (1992).

The performance of the classical 8-node serendipity element, although generally reliable, may deteriorate dramatically under severe mesh distortions. Stiffening effect of mesh distortion leading these elements to poor performance has been known for long (Stricklin *et al.* 1977, Buckland 1978, Gifford 1979, Lee and Bathe 1993, Rajendran and Liew 2000). In practice, the geometric distortions are neither completely avoidable nor always ignorable. Mesh distortions emerge naturally while meshing curved geometries and during large strain nonlinear analysis. Although the ill effects of distortion can be alleviated by reduced integration of element stiffness or through mesh refinement, a rugged element formulation insensitive to mesh distortion is always preferable.

MacNeal and Harder (1992) proposed an improved 8-node isoparametric element, the shape functions of which are obtained by modifying the shape functions of 9-node Lagrangian element. This element reproduces exactly a quadratic displacement field under angular distortions. However, explicit expressions for the modified shape functions have not been derived by MacNeal and Harder (1992). Recently, Kikuchi *et al.* (1999) proposed another 8-node isoparametric element similar to that of MacNeal and Harder (1992), but with explicit expressions for the shape functions. This element also reproduces exactly a quadratic displacement field under angular distortion.

Rajendran and Liew (2003) reported a quadrilateral element (US-QUAD8) that is capable of reproducing a Cartesian quadratic displacement not only under linear and bilinear element geometry but also under quadratic element geometry. This element employs two different sets of shape functions as the basis for the test and trial functions. The distortion-immunity of this formulation under a Cartesian quadratic displacement field crucially depends on a careful choice of the two sets of shape functions.

An important feature of the element proposed by MacNeal and Harder (1992), which is responsible for the better performance of the element, is the use Cartesian quadratic polynomial terms in the shape functions. This motivates the re-investigation of the well-known but less popular element formulation using shape functions directly obtained from the Cartesian polynomial displacement model (e.g., see p116 of Zienkiewicz and Taylor 1989). In order to distinguish them from the parametric shape functions, these shape functions are hereinafter referred to as metric shape functions following MacNeal (1994), and the element developed using such shape functions is called the metric element.

This paper compares the performances of the 8-node metric element, the classical 8-node serendipity element, and the 8-node elements proposed by Kikuchi *et al.* (1999) and Rajendran and Liew (2003) in the presence of mesh distortions. These element types are grouped into four broad

types (viz., parametric, metric, parametric-metric, and metric-parametric) depending on whether the parametric or metric shape functions are used as the basis for test and trial functions. The metric-parametric element refers to a case where the roles of parametric and metric shape functions of USQUAD8 are interchanged. Typical test problems involving severe mesh distortions are solved to assess the relative performance and merits of these element types.

As the performance of elements under different types of mesh distortion is of interest, a classification of various possible distortions is useful. Generally, five types of distortions are encountered with an 8- or 9-node plane element (see. Lee and Bathe 1993), viz., 1) Aspect-ratio distortion, 2) Parallelogram distortion, 3) Angular distortion, 4) Unevenly-spaced-nodes distortion or alternatively called Mid-side node distortion (Rajendran and Liew 2000), and 5) Curved-edge distortion.

For the classification stated above, a square geometry with the mid-side nodes at the centre of their respective sides is treated as the undistorted geometry. A typical element in a distorted mesh may have one or more of the above distortions together. The first distortion type refers to a rectangular element geometry. As the name suggests, the second type refers to parallelogram geometry. The first two types of distortion generally reduce the predictive capability of the overall finite element model as a result of reduced number of elements caused by such distortions. The third type refers to a quadrilateral geometry whereas the fourth type refers to a square element geometry with only the mid-side nodes displaced from their middle position. As the name suggests, the fifth type refers to a square element with one or more curved edges. We will explicitly consider only the last three types of distortion for the present work. The angular distortion commonly appears during mesh generation involving irregular geometries and also in meshing the transition regions between coarse and fine meshes. The curved-edge distortion, as the name suggests, is often encountered in meshing the curved geometries. During nonlinear solution of large strain problems, all the three types of distortion may simultaneously appear.

The mesh distortion may be looked at from the viewpoint of parametric mapping of geometry. Considering a parametric mapping of a bi-unit square in the parameter space to the actual element shape in the Cartesian coordinate space, we note the following:

- a) The aspect ratio distortion or parallelogram distortion is a case of linear (affine) geometric mapping of the form, $x = c_o + c_1\xi + c_2\eta$ and $y = d_o + d_1\xi + d_2\eta$ where c_i and d_i ($i=0, 1$) are arbitrary constants.
- b) The angular distortion corresponds to a bilinear geometric mapping of the form, $x = c_o + c_1\xi + c_2\eta + c_3\xi\eta$ and $y = d_o + d_1\xi + d_2\eta + d_3\xi\eta$.
- c) The mid-side node distortion or curved edge distortion is a case of quadratic geometric mapping of the form, $x = c_o + c_1\xi + c_2\eta + c_3\xi^2 + c_4\eta^2 + c_5\xi\eta^2 + c_6\xi^2\eta$ and $y = d_o + d_1\xi + d_2\eta + d_3\xi^2 + d_4\eta^2 + d_5\xi\eta^2 + d_6\xi^2\eta$.
- d) An element geometry including all the above distortions together corresponds to a quadratic geometric mapping of the form, $x = c_o + c_1\xi + c_2\eta + c_3\xi\eta + c_4\xi^2 + c_5\eta^2 + c_6\xi\eta^2 + c_7\xi^2\eta$ and $y = d_o + d_1\xi + d_2\eta + d_3\xi\eta + d_4\xi^2 + d_5\eta^2 + d_6\xi\eta^2 + d_7\xi^2\eta$.

2. Parametric and metric shape functions

The serendipity parametric shape functions for the 8-node serendipity element are well known in the literature and are reproduced here for convenience:

$$N_i = \frac{1}{4}(1 + \xi\xi_i)(1 + \eta\eta_i)(\xi\xi_i + \eta\eta_i - 1) \quad (1)$$

$$N_j = \frac{1}{2}(1 - \xi^2)(1 + \eta\eta_j) \quad (2)$$

$$N_k = \frac{1}{2}(1 + \xi\xi_k)(1 - \eta^2) \quad (3)$$

where i, j and k refer to the corner nodes, mid-side nodes along η -axis, and mid-side nodes along ξ -axis, respectively. Using these shape functions, the finite element displacement field is interpolated from the nodal displacements as

$$\bar{\mathbf{u}}(x, y) \equiv \begin{Bmatrix} \bar{u}(x, y) \\ \bar{v}(x, y) \end{Bmatrix} = \mathbf{N}\bar{\mathbf{u}}_n \quad (4)$$

where \mathbf{N} and $\bar{\mathbf{u}}_n$ are the shape function matrix and the nodal displacement vector, respectively, defined as

$$\mathbf{N} = \begin{bmatrix} N_1 & 0 & N_2 & 0 & N_3 & 0 & \dots & N_8 & 0 \\ 0 & N_1 & 0 & N_2 & 0 & N_3 & \dots & 0 & N_8 \end{bmatrix} \quad (5)$$

and

$$\bar{\mathbf{u}}_n = [\bar{u}_1, \bar{v}_1, \bar{u}_2, \bar{v}_2, \bar{u}_3, \bar{v}_3, \dots, \bar{u}_8, \bar{v}_8]^T \quad (6)$$

The over-bar and the subscript n in the symbol $\bar{\mathbf{u}}_n$ stand for ‘finite element approximation’ and ‘nodal quantity’, respectively.

The derivation of metric shape functions is well known in the literature but is presented here for convenience of reference. Since there are 8-nodes for the element, the displacement field we ideally want the element to reproduce exactly is written in the form

$$u(x, y) = a_1 + a_2x + a_3y + a_4x^2 + a_5xy + a_6y^2 + a_7x^2y + a_8xy^2 \quad (7)$$

$$v(x, y) = b_1 + b_2x + b_3y + b_4x^2 + b_5xy + b_6y^2 + b_7x^2y + b_8xy^2 \quad (8)$$

where a_i and b_i ($i = 1, 2, 3, \dots, 8$) are arbitrary constants. The first six monomial terms on the right side of Eqs. (7) and (8) correspond to a complete quadratic polynomial. However, the choice of the last two terms is rather arbitrary, as they are just included to make up the number of monomial terms to the number of nodes of the element. For illustrating the procedure to derive the metric shape functions, we now consider only the $u(x, y)$ -displacement. The procedure for $v(x, y)$ -displacement is similar. Eq. (7) is rewritten as

$$u(x, y) = \mathbf{p}^T(x, y)\mathbf{a} \quad (9)$$

where

$$\mathbf{p}^T(x, y) = [1, x, y, x^2, xy, y^2, x^2y, xy^2] \quad (10)$$

and

$$\mathbf{a} = [a_1, a_2, a_3, \dots, a_8]^T \quad (11)$$

Substituting the nodal displacements, $\bar{\mathbf{u}}_i$, and the corresponding nodal coordinates, (x_i, y_i) , for $u(x, y)$ and (x, y) , respectively, in Eq. (9), the following system of eight equations are obtained:

$$\boldsymbol{\phi} = \mathbf{P}\mathbf{a} \quad (12)$$

where

$$\boldsymbol{\phi} = [\bar{u}_1, \bar{u}_2, \bar{u}_3, \dots, \bar{u}_8]^T \quad (13)$$

$$\mathbf{P} = [\mathbf{p}(x_1, y_1), \mathbf{p}(x_2, y_2), \mathbf{p}(x_3, y_3), \dots, \mathbf{p}(x_8, y_8)]^T \quad (14)$$

and

$$\mathbf{p}(x_i, y_i) = [1, x_i, y_i, x_i^2, x_i y_i, y_i^2, x_i^2 y_i, x_i y_i^2]^T \quad (15)$$

Assuming that the geometry of the element is such that \mathbf{P}^{-1} exists, Eq. (12) is solved for \mathbf{a} as

$$\mathbf{a} = \mathbf{P}^{-1}\boldsymbol{\phi} \quad (16)$$

Using Eq. (16) in (9),

$$u(x, y) = (\mathbf{p}^T(x, y)\mathbf{P}^{-1})\boldsymbol{\phi} = \mathbf{m}^T\boldsymbol{\phi} \quad (17)$$

where the metric shape functions, M_i , are defined as

$$\mathbf{m}^T \equiv [M_1, M_2, M_3, \dots, M_8] \equiv \mathbf{p}^T(x, y)\mathbf{P}^{-1} \quad (18)$$

Eq. (18) may also be rewritten as

$$\mathbf{m} \equiv [M_1, M_2, M_3, \dots, M_8]^T \equiv \mathbf{P}^{-T}\mathbf{p}(x, y) \quad (19)$$

Analogous to Eq. (4), the finite element displacement field is written in terms of the metric shape functions as

$$\bar{\mathbf{u}}(x, y) \equiv \begin{Bmatrix} \bar{u}(x, y) \\ \bar{v}(x, y) \end{Bmatrix} = \mathbf{M}\bar{\mathbf{u}}_n \quad (20)$$

where \mathbf{M} is a matrix of metric shape function matrix defined as

$$\mathbf{M} = \begin{bmatrix} M_1 & 0 & M_2 & 0 & M_3 & 0 & \dots & M_8 & 0 \\ 0 & M_1 & 0 & M_2 & 0 & M_3 & \dots & 0 & M_8 \end{bmatrix} \quad (21)$$

2.1 The continuity and completeness requirements of shape functions

The continuity requirement for the plane stress/strain application of the 8-node element is that the displacement model must satisfy the intra- and inter-element continuity at least to a level of C^1 and C^0 , respectively. The metric shape functions as well as the parametric shape functions do satisfy the minimum requirement of C^1 intra-element continuity. However, the case with inter-element continuity is different: The metric shape functions satisfy the inter-element continuity along the element edges if the element geometry is square or rectangle but not in general for arbitrary geometries. On the other hand, the parametric shape functions satisfy the inter-element continuity along the element edge for any arbitrary but admissible geometry. An admissible geometry is one for which the determinant of Jacobian matrix (associated with the transformation between global Cartesian and the local parametric coordinates) is positive.

In the literature, the completeness requirements are usually associated with the ability of the element shape functions to reproduce an arbitrary linear polynomial displacement field of the form $u(x, y) = a_1 + a_2x + a_3y$ and $v(x, y) = b_1 + b_2x + b_3y$. For this reason, these completeness requirements will hereinafter be referred to as the linear completeness requirements which demand the following conditions to be satisfied by the element shape functions, ψ_i , at any point inside the element:

$$\sum_{i=1}^8 \psi_i = 1 \quad (22)$$

$$\sum_{i=1}^8 \psi_i x_i = x \quad (23)$$

$$\sum_{i=1}^8 \psi_i y_i = y \quad (24)$$

The linear completeness requirements ensure that the finite element solution converges to the exact solution in the limit of mesh refinement. However, higher order elements are often used in practice in order to get an accurate solution with fewer elements. The linear completeness requirements are no longer sufficient as they can only ensure convergence to correct solution only in the limit of mesh refinement. Thus, for the effective use of higher order elements, it is necessary to investigate the higher order completeness requirements of shape functions. Rajendran and Liew (2000) discuss the higher order completeness requirements for the 8-node plane element. Arnold *et al.* (2002) provide a function space interpretation of such conditions. For an 8-node plane element to reproduce a quadratic displacement field given by Eqs. (7) and (8), the following conditions are to be satisfied in addition to Eqs. (22)-(24):

$$\sum_{i=1}^8 \psi_i x_i^2 = x^2 \quad (25)$$

$$\sum_{i=1}^8 \psi_i x_i y_i = xy \quad (26)$$

$$\sum_{i=1}^8 \psi_i y_i^2 = y^2 \tag{27}$$

$$\sum_{i=1}^8 \psi_i x_i^2 y_i = x^2 y \tag{28}$$

$$\sum_{i=1}^8 \psi_i x_i y_i^2 = x y^2 \tag{29}$$

Eqs. (22)-(29) may be written concisely as

$$\mathbf{P}^T \boldsymbol{\psi} = \mathbf{p}(x, y) \tag{30}$$

where

$$\boldsymbol{\psi} = [\psi_1, \psi_2, \psi_3, \dots, \psi_8]^T \tag{31}$$

From Eq. (30),

$$\boldsymbol{\psi} = \mathbf{P}^{-T} \mathbf{p}(x, y) \tag{32}$$

Comparing Eqs. (19) and (32), we observe that $\boldsymbol{\psi} \equiv \mathbf{m}$, which means that the metric shape functions, M_i , satisfy all the completeness requirements (Eqs. (22)-(29)) inherently. Note that this observation holds even for the distorted element geometry as long as \mathbf{P}^{-1} exists. However, the parametric shape functions, N_i , do not satisfy all the completeness requirements, in particular Eqs. (25)-(29), for all geometries. It is easy to verify that the parametric shape functions do satisfy Eq. (22). Eqs. (23) and (24) are also satisfied implicitly by isoparametric formulations because these equations themselves form the basis of geometry interpolation. Satisfaction of Eqs. (25)-(29), however, depends on the geometrical shape of the element. For example, for rectangular geometries with the sides parallel to the global Cartesian coordinate axes and the mid-side nodes positioned at the centre of the sides, i.e., for linear (affine) geometries, the parametric shape functions satisfy all the Eqs. (25)-(29). For an arbitrarily oriented rectangular geometry with the mid-side nodes at the centre of the sides or a parallelogram geometry with the mid-side nodes at the centre of the sides, the parametric shape functions satisfy Eqs. (25)-(27), and not Eqs. (28) and (29) in general. For an arbitrary quadrilateral geometry or an arbitrary geometry with curved edges, Eqs. (25)-(29) are not satisfied. Table 1 shows a comparison of parametric and metric shape functions with respect to satisfaction of continuity and completeness requirements.

Table 1 Continuity and completeness of parametric and metric shape functions

Shape function type	Satisfaction of inter-element (C^0) and intra-element continuity (C^1)	Satisfaction of higher order completeness, Eqs. (25)-(29)
Parametric	For all admissible geometry	[#] Not for all admissible geometry
Metric	[#] Not for all admissible geometry	For all admissible geometry

[#]Satisfied for special geometries like square/rectangle/parallelogram with sides parallel to global coordinate axes.

The above observations have important implications in the choice of shape functions for an element. If we want the shape functions satisfy the higher order completeness requirements (Eqs. (25)-(29)), the metric shape functions offer a better choice compared to the parametric shape functions. However, if we want the elements to satisfy the inter-element compatibility, the parametric shape functions emerge to be a better choice. Thus, the two sets of shape functions play the complementary roles. Ideally, we want shape functions that satisfy both requirements. However, such shape functions are hard to obtain for this element. Rajendran and Liew (2003) have observed that the parametric shape functions serve as a good choice for constructing the test functions, and the metric shape functions for the trial functions. The element formulated so (US-QUAD8) performs well under distorted mesh. Motivated by this observation, the following four element formulations are explored in the rest of the paper for an insight into how the choice of basis for test and trial functions affects the element performance:

2.2 Parametric element (PP element)

This is the same as the classical 8-node isoparametric serendipity element (QUAD8) using the shape functions given by Eqs. (1)-(3) for both test and trial functions. The element stiffness matrix, load vector due to body forces and that due to surface forces are computed as usual using the equations,

$$\mathbf{K}^{(e)} = \int_{V^{(e)}} (\mathbf{LN})^T \mathbf{D} (\mathbf{LN}) dV^{(e)} \quad (33)$$

$$\mathbf{f}_b^{(e)} = \int_{V^{(e)}} \mathbf{N}^T \mathbf{b}^{(e)} dV^{(e)} \quad (34)$$

$$\mathbf{f}_t^{(e)} = \int_{V^{(e)}} \mathbf{N}^T \mathbf{t}^{(e)} dV^{(e)} \quad (35)$$

respectively, where \mathbf{L} and \mathbf{D} are the usual strain-displacement differential operator matrix, and the material constitutive matrix, respectively, and $\mathbf{b}^{(e)}$ and $\mathbf{t}^{(e)}$ are body and surface forces, respectively.

2.3 Metric element (MM element)

For this element, the metric shape functions given by Eq. (21) are used for the test and trial functions. Recently, Rajendran and Liew (2002) have tested the performance of this element under mesh distortion. The element stiffness matrix and the load vectors for this element are computed as

$$\mathbf{K}^{(e)} = \int_{V^{(e)}} (\mathbf{LM})^T \mathbf{D} (\mathbf{LM}) dV^{(e)} \quad (36)$$

$$\mathbf{f}_b^{(e)} = \int_{V^{(e)}} \mathbf{M}^T \mathbf{b}^{(e)} dV^{(e)} \quad (37)$$

$$\mathbf{f}_t^{(e)} = \int_{V^{(e)}} \mathbf{M}^T \mathbf{t}^{(e)} dV^{(e)} \quad (38)$$

2.4 Parametric-metric element (PM element)

This element uses parametric shape functions and metric shape functions used as the test and trial functions, respectively, and is the same as the US-QUAD8 element of Rajendran and Liew (2003). This formulation may be looked upon as a typical Petrov-Galerkin formulation where different sets of basis functions are used for the test and trial functions. The element stiffness matrix and the load vectors for this element become

$$\mathbf{K}^{(e)} = \int_{V^{(e)}} (\mathbf{LN})^T \mathbf{D} (\mathbf{LM}) dV^{(e)} \tag{39}$$

$$\mathbf{f}_b^{(e)} = \int_{V^{(e)}} \mathbf{N}^T \mathbf{b}^{(e)} dV^{(e)} \tag{40}$$

$$\mathbf{f}_t^{(e)} = \int_{V^{(e)}} \mathbf{N}^T \mathbf{t}^{(e)} dV^{(e)} \tag{41}$$

2.5 Metric-parametric element (MP element)

This element also uses two different sets of basis functions but with the roles of parametric shape functions and metric shape functions interchanged. For this element, the stiffness matrix and the load vectors become

$$\mathbf{K}^{(e)} = \int_{V^{(e)}} (\mathbf{LM})^T \mathbf{D} (\mathbf{LN}) dV^{(e)} \tag{42}$$

$$\mathbf{f}_b^{(e)} = \int_{V^{(e)}} \mathbf{M}^T \mathbf{b}^{(e)} dV^{(e)} \tag{43}$$

$$\mathbf{f}_t^{(e)} = \int_{V^{(e)}} \mathbf{M}^T \mathbf{t}^{(e)} dV^{(e)} \tag{44}$$

The PP and MM elements conform to Galerkin formulation and thus results in symmetric stiffness matrix because the same set of shape functions is used on the right as well as left side of the **D** matrix in the stiffness integral in Eqs. (33) and (36). However, the PM and MP elements conform to Petrov-Galerkin formulation and results in an unsymmetric stiffness matrix because of different sets of shape functions used. For solving test problems of section 3, the element geometry is interpolated using the parametric shape functions (Eqs. (1)-(3)) for each of the four formulations. Thus, there are

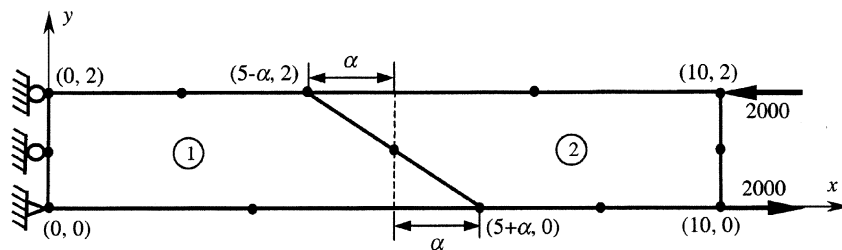
Table 2 Choice of shape functions for the four element formulations studied in this paper

Element type	Left shape functions	Right shape functions	Geometry interpolation
Parametric (PP)	Parametric	Parametric	Parametric
Metric (MM)	Metric	Metric	Parametric
Parametric-metric (PM)	Parametric	Metric	Parametric
Metric-parametric (MP)	Metric	Parametric	Parametric

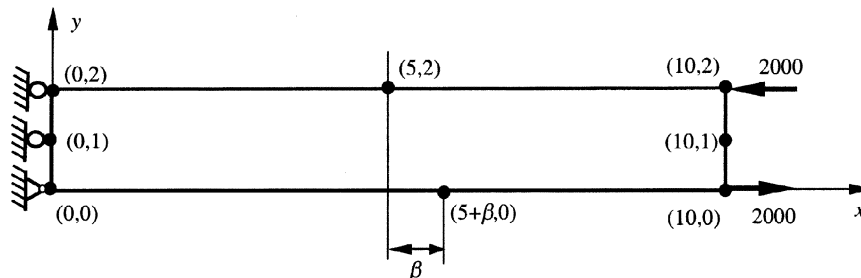
three generic roles of shape functions, viz., (i) as left shape functions to represent the test function, (ii) as right shape functions to represent the trial function, and (iii) as interpolation functions for geometry. Table 2 provides a summary of the choice of shape functions with respect to these three roles for the four element formulations mentioned above.

3. Test problems

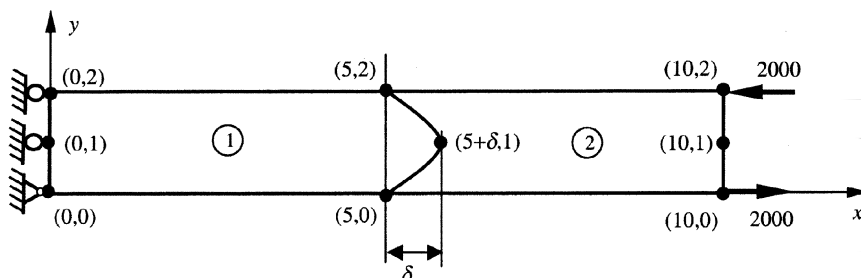
The performances of the four element types discussed in section 2 are studied for typical test problems involving mesh distortion. All the four elements perform equally well for meshes involving square or rectangular element geometries. However, they show marked difference in performance under mesh distortion, which forms the focus of the present paper. The numerical integration of stiffness matrix is carried out using a 3×3 Gaussian quadrature unless stated otherwise.



(a) A two-element mesh with angular distortion.



(b) A single-element mesh with mid-side node distortion.



(c) A two-element mesh with curved-edge distortion.

Fig. 1 Distorted meshes for the cantilever beam under pure bending

3.1 Test Problem no. 1: A cantilever beam under pure bending

This test problem is same as the test problem no. 2 of Rajendran and Liew (2000). A cantilever beam of length, $L = 10$, depth, $d = 2$, and thickness, $t = 2$, is restrained at one end and a bending moment, $M = 4000$, is applied at the tip. The units for the numerical values quoted in this paper are not explicitly stated; consistent units are assumed. The beam is modelled using two 8-node plane elements belonging to the four types of formulation discussed in section 2. Young's modulus, E , and Poisson's ratio, γ , are taken as 1500 and 0.25, respectively. The bending moment is represented by two equal and opposite forces of 2000 units magnitude as shown in Fig. 1. The exact solution for this problem by the classical beam theory gives a tip displacement, $ML^2/2EI = 100$, and a bending stress, $\pm Md/2I = \pm 3000$, for the bottom and top surfaces of the beam, respectively. This problem involves a quadratic displacement field. A quadratic displacement field can in general be reproduced by quadratic elements under aspect ratio and parallelogram distortions, and therefore these distortions are not considered here.

3.1.1 A two-element mesh with angular distortion

A two-element mesh with angular distortion as shown in Fig. 1(a) is considered. The extent of angular distortion is controlled by varying the parameter, α . While varying the angular distortion, the mid-side nodes are re-positioned at the mid-point of the respective sides. The computed nodal displacements at (10, 2) are plotted in Fig. 2(a). The results with the 8-node element of Kikuchi *et al.* (1999) are also shown for comparison. Fig. 2(a) shows that PM and MP elements, and the element of Kikuchi *et al.* (1999) are able to reproduce the exact displacement solution irrespective of the value of distortion parameter. The MM element performs reasonably well with a typical error of about 5% for $\alpha = 4.0$. The PP element exhibits the highest sensitivity to mesh distortion with an error of about 66% for $\alpha = 4.0$.

The computed nodal σ_x -stress at $(5 - \alpha, 2)$ is plotted in Fig. 2(b) which shows that the PM element as well as that of Kikuchi *et al.* (1999) is able to reproduce the exact stress solution irrespective of the magnitude of distortion. The MM element performs reasonably well and its

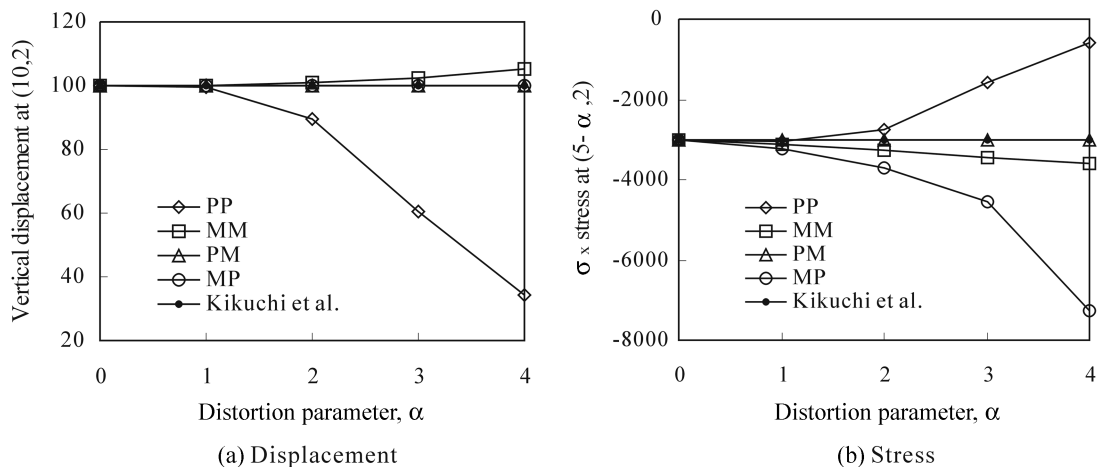


Fig. 2 Sensitivity to angular distortion

performance is better than that of the MP element as well as that of the PP element. The performance of PP element is again poor with an error of about 80% for $\alpha = 4.0$. The MM element discussed here is the same as Formulation 2 discussed in section 3.2 of Rajendran and Liew (2000). However, it should be noted that the results shown in the Tables 7 and 8 of this reference are in error, and therefore do not agree with the results of Figs. 2(a) and 2(b), respectively.

3.1.2 A single element mesh with mid-side node distortion

The cantilever beam is then modelled with a single element having mid-side node distortion as shown in Fig. 1(b). The extent of mesh distortion is varied by moving the mid-side node at the bottom edge of the element by a distance, β , in the positive x -direction. All the other nodes are kept at their original locations. The displacement and stress values computed for typical values of β are shown in Figs. 3(a) and 3(b), respectively. It is seen from these figures that the MM and PM

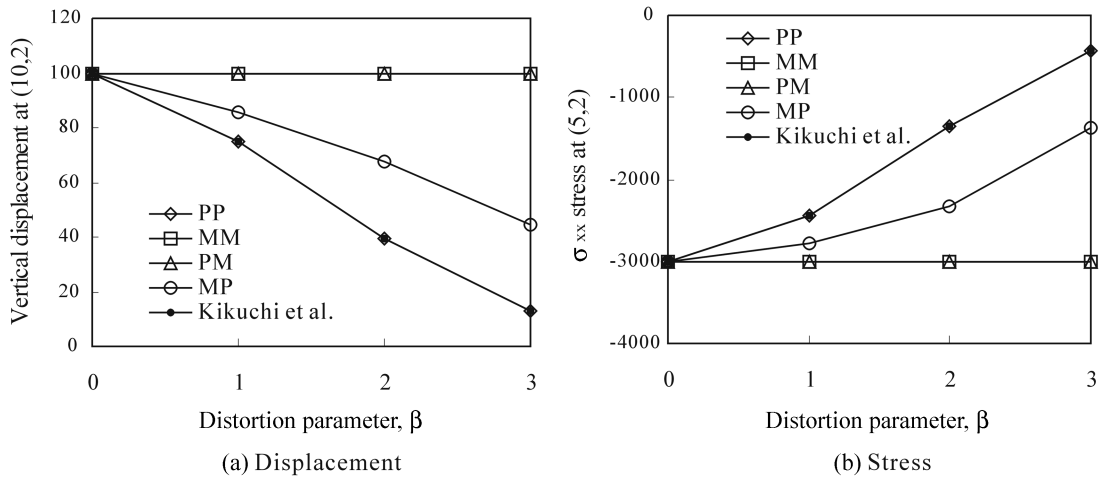


Fig. 3 Sensitivity to mid-side node distortion

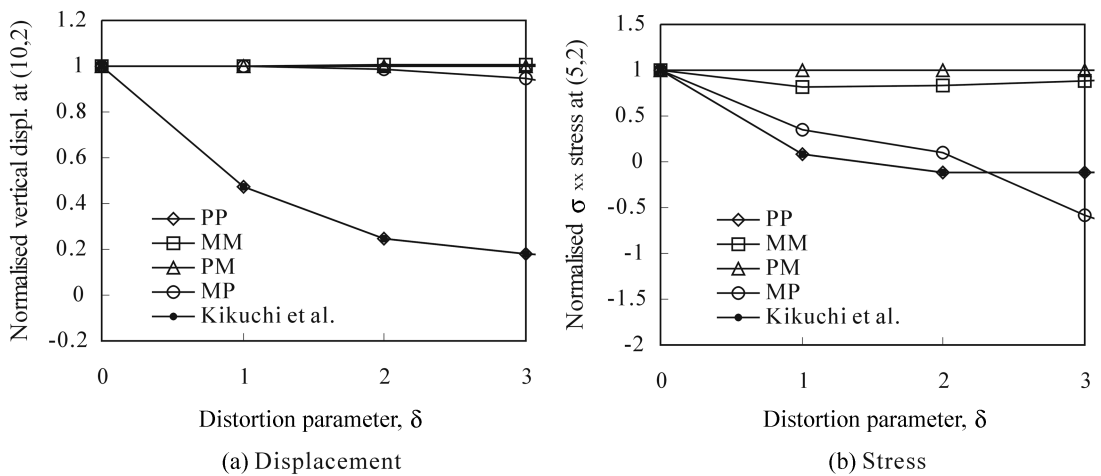


Fig. 4 Sensitivity to curved-edge distortion

elements are able to reproduce the exact displacement and stress solution for all values of β . The results for the 8-node element of Kikuchi *et al.* (1999) are the same as for the PP element. Although the 8-node element of Kikuchi *et al.* (1999) has been able to reproduce exact solution under angular distortion (Fig. 2), its performance under mid-side node distortion is thus bad, and similar to that of the PP element.

3.1.3 Two-element mesh with quadratic curved-edge distortion

The cantilever beam is then modelled with a two-element mesh having quadratic curved-edge distortion. The magnitude of curved-edge distortion is controlled by varying the x -coordinate of the mid-side node (Fig. 1(c)), which is otherwise located at (5,1). The computed displacement and stress values for typical values of distortion parameter, δ , are shown in Fig. 4. Only the PM element is able to reproduce the exact displacement as well as stress for this mesh. MM element is the next best performing element. The performance of other elements are poor, particularly with respect to the stress results.

Thus, with respect to all the three types of distortion considered, only PM element is capable of reproducing the exact displacement and stress.

3.1.4 A severely distorted mesh

A mesh that has all the above three types of distortions together is considered here. In manufacturing processes involving large strains, such as forging, deep drawing, extrusion, etc., various distortions could arise simultaneously, and hence the study of performance of elements

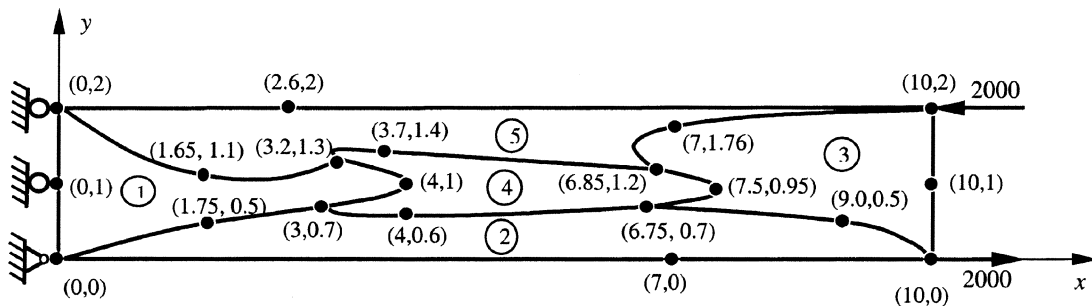


Fig. 5 A severely distorted mesh involving simultaneously three types of distortion, viz., angular distortion, mid-side node distortion and curved-edge distortion

Table 3 Computed results for Problem 1 under severely distorted mesh (3 × 3 integration)

	PP element	MM element	PM element	MP element	8-node element of Kikuchi <i>et al.</i> (1999)
# σ_x at (0,0)	134	3017	3000	6213	74
# σ_x at (0,2)	10	-2567	-3000	-447	46
v at (10,2)	8.62	101.38	100	149.52	8.49
Exact solution:	σ_x at (0,0) = 3000;		σ_x at (0,2) = -3000;		v at (10,2) = 100

#Calculated with respect to element No. 1

under combined distortions is of considerable practical significance. The problem considered is again the same as shown in Fig. 1, but the finite element mesh has five elements as shown in Fig. 5 that includes simultaneously various distortions, viz., angular distortion, mid-side node distortion and curved-edge distortion. The lines defining the element boundaries shown in Fig. 5 have been plotted by the parametric interpolation. Typical displacement and stress results for this mesh are shown in Table 3. The PM element is able to reproduce the exact displacements and stresses notwithstanding the severity of distortion. The PP element, MP element, and the 8-node element of Kikuchi *et al.* (1999) produce results that deviate far from the exact solution. The performance of MM element is far better, though not exact.

The problem was also solved using the PLANE82 element of the commercial finite element package, ANSYS5.4. A reduced 2×2 integration is used by ANSYS5.4 for the computation of stiffness matrix (Kohnke 1997), and hence for comparison purposes, the displacement and stress results of the five element types shown in Table 3 have been re-computed with 2×2 integration.

Table 4 Computed results for Problem 1 under severely distorted mesh (2×2 integration)

	PP element	MM element	PM element	MP element	8-node element of Kikuchi <i>et al.</i> (1999)	PLANE82 element (ANSYS5.4)
# σ_x at (0,0)	249	4176	2570	3729	175	266
# σ_x at (0,2)	-329	-5282	-2741	666	-56	-1001
v at (10,2)	16.18	114.32	100.49	109.94	17.96	16.18
Exact solution:	σ_x at (0,0) = 3000;		σ_x at (0,2) = -3000;		v at (10,2) = 100	

#Calculated with respect to element No. 1

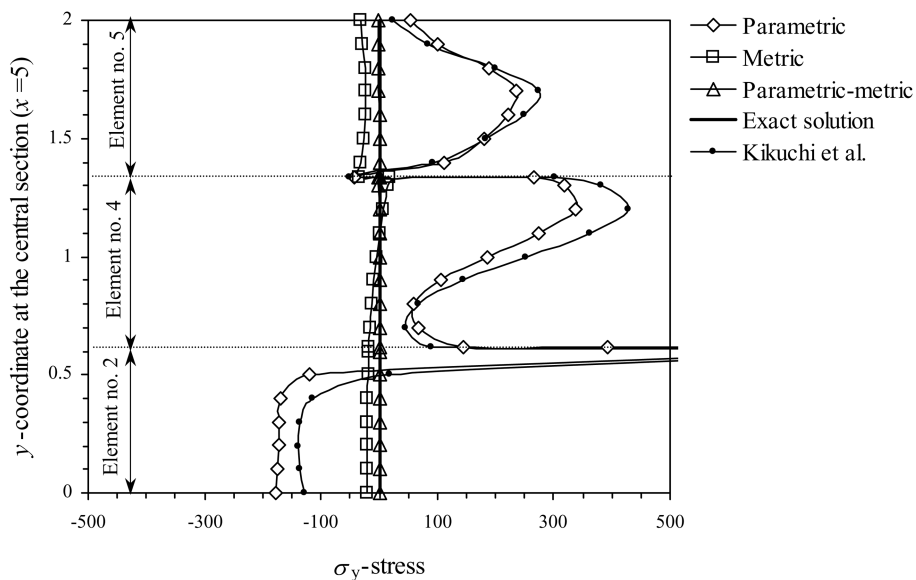


Fig. 6 σ_x -stress distribution across the mid-section of the beam for the severely distorted mesh shown in Fig. 5

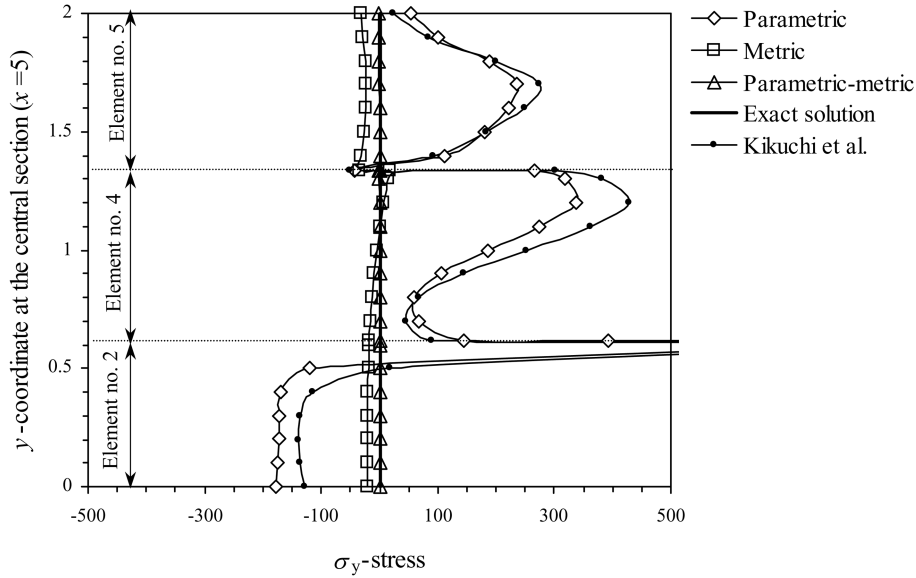


Fig. 7 σ_y -stress distribution across the mid-section of the beam for the mesh shown in Fig. 5

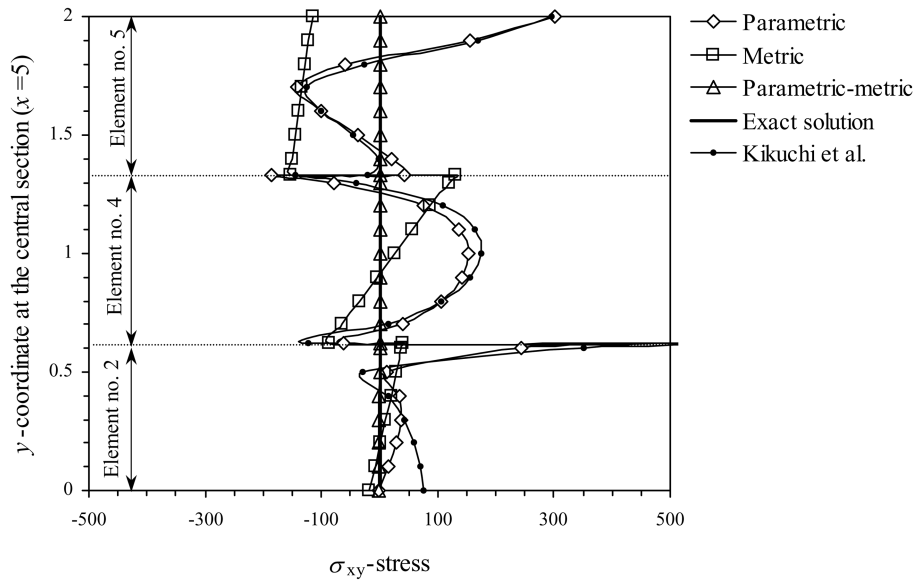


Fig. 8 σ_{xy} -stress distribution across the mid-section of the beam for the mesh shown in Fig. 5

The results are summarised in Table 4, which suggest that even with reduced integration, the PM element produces the best results though not exact as in Table 3.

The distribution of σ_x stress across the mid-section ($x = 5$) of the beam is shown in Figs. 6-8. (The y -coordinates, and the ξ - and η -coordinates of the points at which the stresses are computed are listed in Table 5 for reference purposes. The values of ξ and η are the roots of the two simultaneous

Table 5 Coordinates of points at the mid-section of mesh shown in Fig. 5 at which the stresses are computed

y	PP, MM, PM and MP elements		8-node isoparametric element of Kikuchi <i>et al.</i> (1999)	
	ξ	η	ξ	η
0.0	-0.350781	-1.000000	-0.350781	-1.000000
0.1	-0.348040	-0.827647	-0.332033	-0.821532
0.2	-0.339936	-0.637266	-0.306036	-0.623719
0.3	-0.322435	-0.421286	-0.267691	-0.398285
0.4	-0.285595	-0.164495	-0.205124	-0.128798
0.5	-0.194422	0.174491	-0.081424	0.226702
0.55	-0.078467	0.420131	0.044283	0.474891
0.6	0.240434	0.813085	0.291795	0.826964
0.61	0.342744	0.909888	0.364992	0.913637
0.61954	0.442047	0.999939	0.442144	1.000031
0.61955	0.442110	-0.999989	0.442105	-0.999980
0.7	0.329390	-0.764279	0.330560	-0.765003
0.8	0.234550	-0.497756	0.236662	-0.498905
0.9	0.184416	-0.241703	0.186961	-0.243014
1.0	0.180704	0.013628	0.183160	0.012336
1.1	0.224674	0.275409	0.226594	0.274315
1.2	0.315234	0.554034	0.316355	0.553317
1.3	0.455329	0.872802	0.455596	0.872607
1.33393	0.517769	1.000088	0.517755	1.000042
1.33393	0.517785	-0.999889	0.517773	-0.999897
1.4	0.612983	-0.773169	0.601051	-0.775277
1.5	0.666203	-0.515846	0.649982	-0.512897
1.6	0.675467	-0.258316	0.656574	-0.249546
1.7	0.646865	0.037304	0.625657	0.051867
1.8	0.576517	0.386397	0.557081	0.399799
1.9	0.483900	0.729593	0.473777	0.733328
2.0	0.398155	1.000000	0.402311	0.999998

nonlinear equations, $f_1(\xi, \eta) \equiv x - \sum_{i=1}^8 N_i x_i = 0$ and $f_2(\xi, \eta) \equiv y - \sum_{i=1}^8 N_i y_i = 0$, with $x = 5$ and y -values listed in Table 5, which have been solved using the Mathematica software. N_i in these two equations are shape functions as defined in Eqs. (1)-(3) for PP, MM, PM and MP elements, and as given by Kikuchi *et al.* (1999) for the 8-node element of Kikuchi *et al.* The stress values shown in Figs. 6-8 are computed with 3×3 integration of stiffness matrix. It is seen from Fig. 6 that the MM element and the PM element are able to represent the linear distribution of σ_x -stress accurately. The PM element reproduces the exact solution whereas the MM element has small errors although not visible in the current scale of plot in Fig. 6. The error is about 2.4% and 0.4% at the top and bottom surfaces of the beam. The PP element, MP element and that of Kikuchi *et al.* (1999) are not successful in representing the linear variation of σ_x -stress. The MP element exhibits violent fluctuation of stress across the cross section. Figs. 7 and 8 show the distribution of σ_y - and σ_{xy} -

stresses, respectively. The results of MP element exhibits too violent fluctuation to be accommodated in the current scale of the plots, and hence not shown in these figures. Figs. 7 and 8 show that only the PM element is able to correctly represent the exact distribution of zero σ_y - and σ_{xy} -stresses across the cross section.

3.2 Test Problem no. 2: A cantilever beam with a parabolic shear force at the tip

A cantilever beam of length, $L = 10$, depth, $d = 2$, and thickness, $t = 1$, is fixed at one end and a parabolically distributed shear force, $P = 300$, is applied at the tip. Young's modulus, E , and Poisson's ratio, γ , are taken as 1500 and 0.25, respectively. The finite element mesh is shown in Fig. 9, which is same as in Fig. 5, but with different boundary and loading conditions. The exact solution for this problem is given by Timoshenko and Goodier (1934)

$$u = -\frac{P(L-x)^2(y-d/2)}{2EI} - \frac{\gamma P(y-d/2)^3}{6EI} + \frac{P(y-d/2)^3}{6IG} + \left(\frac{Pl^2}{2EI} - \frac{P(d/2)^2}{2IG}\right)(y-d/2) \tag{45}$$

$$v = \frac{\gamma P(L-x)(y-d/2)^2}{2EI} + \frac{P(L-x)^3}{6EI} - \frac{Pl^2(L-x)}{2EI} + \frac{Pl^3}{3EI} \tag{46}$$

$$\sigma_x = -\frac{P(L-x)(y-d/2)}{I} \tag{47}$$

$$\sigma_y = 0 \tag{48}$$

$$\sigma_{xy} = \frac{Py}{2I}(d-y) \tag{49}$$

where $G = E/2(1 + \gamma)$ is the rigidity modulus. For this solution to be valid, normal and shearing forces conforming to Eqs. (47) and (49) must be applied at the fixed-edge.

In the finite element model, the parabolic shear force is represented by three consistently lumped nodal forces, 30, 240 and 30, acting upwards at the tip as shown in Fig. 9. Vertical lumped forces of -30 and -240 are applied at the nodes at (0,2) and (0,1), respectively, conforming to Eq. (49). The

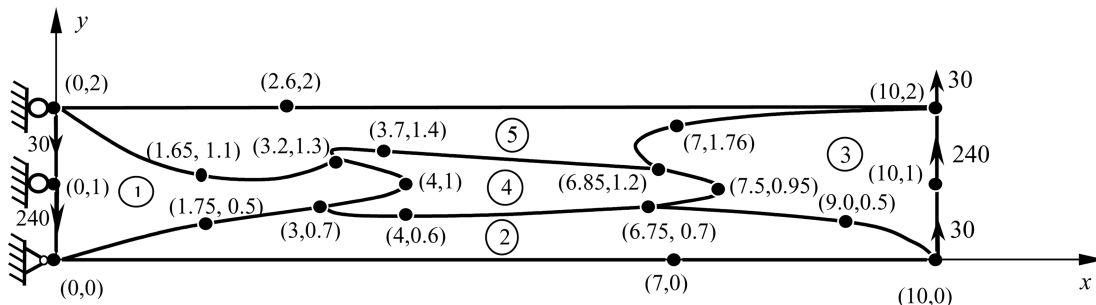


Fig. 9 A severely distorted mesh for a cantilever beam with a parabolically distributed tip shear force

Table 6 Computed results for Problem 2 under severely distorted mesh (3×3 integration)

	PP element	MM element	PM element	MP element	8-node element of Kikuchi <i>et al.</i> (1999)
# $\sigma_x(0,0)$	130	3464	4426	8118	185
# $\sigma_x(0,2)$	213	-3044	-4100	4317	312
$v(10,2)$	11.39	89.12	118.39	126.05	12.18
Exact solution:	σ_x at (0,0) = 4500;		σ_x at (0,2) = -4500;		v at (10,2) = 100

#Calculated with respect to element No. 1

Table 7 Computed results for Problem 2 under severely distorted mesh (2×2 integration)

	PP element	MM element	PM element	MP element	8-node element of Kikuchi <i>et al.</i> (1999)	PLANE82 element (ANSYS5.4)
# $\sigma_x(0,0)$	333	9328	7499	7730	405	169
# $\sigma_x(0,2)$	158	-7602	-5579	13030	454	-1009
$v(10,2)$	20.03	114.76	103.53	100.69	22.12	18.99
Exact solution:	σ_x at (0,0) = 4500;		σ_x at (0,2) = -4500;		v at (10,2) = 100	

#Calculated with respect to element No. 1

nodes at (0,1) and (0,2) are restrained in the x -direction, and the node at (0,0) is restrained in both x - and y -directions. These boundary conditions automatically produce the necessary normal forces (as reactions) that conform to lumped forces otherwise obtainable from Eq. (47).

The computed displacements and stresses are summarised in Table 6. None of the elements is able to reproduce the exact solution as the exact displacement solution (Eqs. (45) and (46)) is an incomplete cubic polynomial in (x, y) which is one order higher than what any of the five types of elements can at best reproduce. It is seen from Table 6, the PP element and the 8-node element of Kikuchi *et al.* (1999) exhibit poorer performance. The stress value $\sigma_x(0,2)$ given by these two elements as well as that given by MP element are positive in sign whereas the exact stress value is negative. The MM element and MP element exhibit a somewhat better performance than these two elements. The stress results of PM element are better than that of MM element. Table 7 shows the results for this problem with reduced integration of stiffness matrix. Here again, the PP element and the 8-node element of Kikuchi *et al.* (1999) exhibit poorer performance. The displacement given by PLANE82 element of ANSYS5.4 is comparable to that of these two elements. MP element gives the most accurate displacement value, although it gives an erroneous positive value of 13030 for $\sigma_x(0,2)$. The results of MM element and the PM elements are somewhat comparable to the exact solution. The signs of stress values given by these two elements are correct although the magnitudes are higher than the exact value.

The distribution of stresses across the mid-section of the beam is shown in Figs. 10-12. Here again, the stress values are computed with 3×3 stiffness integration. It is seen from Fig. 10 that the MM and PP elements are able to represent the linear distribution of bending stress (σ_x -stress) whereas the other elements, in particular the MP element, exhibits considerable deviations from linear distribution. The σ_x -stress results of MM element match exact solution very closely, with small errors that are not visible in this scale of the plot. The PM element exhibits significant

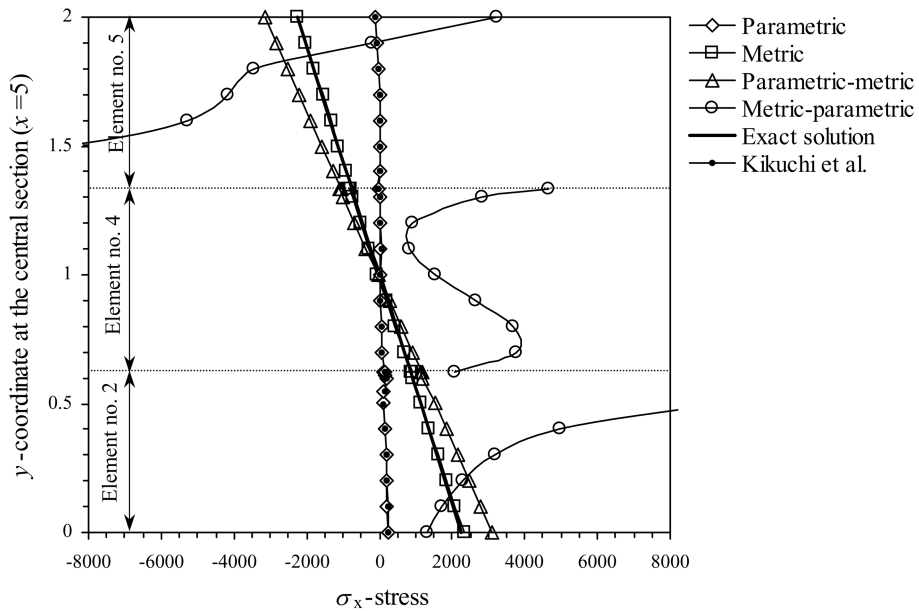


Fig. 10 σ_x -stress distribution across the mid-section of the beam for the mesh shown in Fig. 9

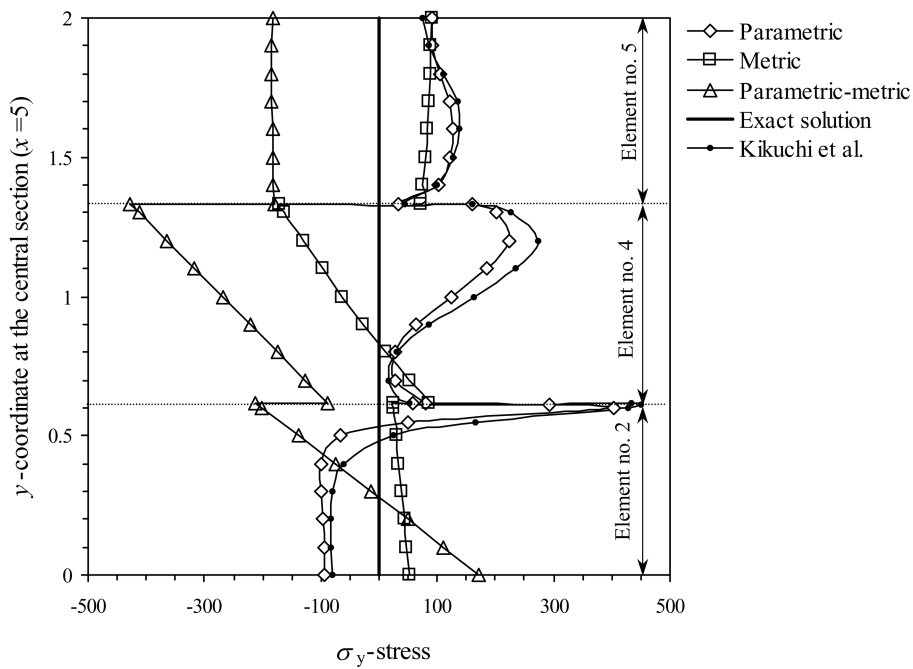


Fig. 11 σ_y -stress distribution across the mid-section of the beam for the mesh shown in Fig. 9

deviation from the exact solution. It is seen from Fig. 11 that none of the elements is able to represent the zero distribution of σ_y -stress. It is seen from Fig. 12, none of the elements is able to

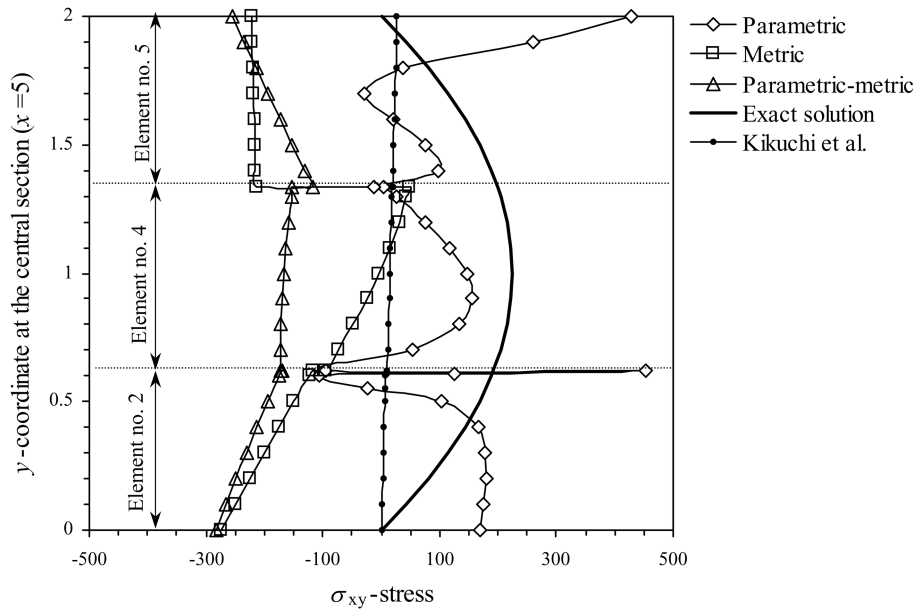


Fig. 12 σ_{xy} -stress distribution across the mid-section of the beam for the mesh shown in Fig. 9

Table 8 Reproduceability of quadratic displacement field under distorted mesh

Element geometry /Distortion type	PP element	MM element	PM element	MP element	8-node element of Kikuchi <i>et al.</i> (1999)
Linear geometry:					
Aspect ratio distortion	yes	yes	yes	yes	yes
Parallelogram distortion	yes	yes	yes	yes	yes
Bilinear geometry:					
Angular distortion	no	no	yes	no	yes
Quadratic geometry:					
Mid-side node distortion	no	yes	yes	no	no
Curved-edge distortion	no	no	yes	no	no

match the parabolic distribution of σ_{xy} -stress. The distribution given by the PM element somewhat resembles a parabola in a piece-wise sense although it is shifted leftward with respect to the exact distribution. The distribution of stresses within each element domain as given by the MM and PM elements is linear whereas that of the PP element and the element of Kikuchi *et al.* (1999) are nonlinear.

3.3 Some general comments on the four formulations of section 2

The PP and MM formulations are well known in the literature, and the PM and MP formulations are obscure. Although the PP and MM formulations are already known, the PP formulation has

been preferentially used and advocated for certain reasons such as that it yields a compatible or conforming element. Degeneration of the isoparametric quadrilateral element to a triangular element by collapsing the three nodes of a side works with PP formulation while, in MM or PM or MP formulation, it leads to singularity of \mathbf{P} matrix due to repeated coordinates of the collapsed nodes.

The PM element is an incompatible element because it uses metric shape functions to construct trial function, which are not compatible for all element geometries. However, the ill effects of incompatibility do not show up if the element is used under linear or quadratic displacement fields. Furthermore, it is capable of reproducing a quadratic displacement field even under extreme mesh distortions as long as the Jacobian of geometric mapping is unique at the quadrature points. Table 8 gives a summary of reproduceability of quadratic displacement field by various elements under linear, bilinear and quadratic mesh distortions.

The PP formulation has been the staple formulation in finite element literature. Although the shape functions used in the PP element satisfy interelement continuity, they do not satisfy Cartesian quadratic completeness under general distorted geometries, which causes the distortion sensitivity under a quadratic displacement field.

The MM formulation, although known for long and is often presented in textbooks for simpler elements like the CST triangle, has been unpopular for 8-node quadrilateral element. Although the shape functions used in MM element satisfy Cartesian quadratic completeness under general distorted geometries, it does not satisfy inter-element continuity, which prevents reproduction of quadratic displacement fields under distorted meshes.

The PM formulation uses two different sets of shape functions for constructing test and trial functions. The left (test) shape functions are chosen to satisfy the interelement continuity, and the right (trial) shape functions are chosen to satisfy the Cartesian quadratic completeness. This particular choice is identified to be responsible for the distortion-immune performance of the PM element under quadratic displacement fields (Rajendran and Liew 2003).

The MP formulation is similar to PM formulation, but the roles of left and right shape functions are interchanged although there is no theoretical justification to do so. However, this element is useful to demonstrate that the distortion immunity in PM element is not fortuitous and an arbitrary choice of shape functions as in MP element does not lead to distortion-immune performance.

4. Conclusions

The performances of four types of formulations of 8-node plane quadratic element, viz., parametric (PP), metric (MM), parametric-metric (PM) and metric-parametric (MP) formulations, have been compared in the presence of mesh distortion. The PP and MM formulations are already well known in the literature, and they use the same set of shape functions as the basis functions for the test and trial functions. The PM and MP formulations use different sets of shape functions as the basis functions for the test and trial functions. The numerical test results reveal that the PP formulation, on which the classical 8-node serendipity element is based, leads to poor results under severely distorted meshes. The MM and PM formulations perform superior to other formulations. The PM element is able to reproduce a quadratic displacement field even under extreme mesh distortions where the other elements are not. This element also performs acceptably well under reduced integration of stiffness matrix.

References

- Arnold, D.N., Boffi, D. and Falk, R.S. (2002), "Approximation by quadrilateral finite elements", *Mathematics of Computation*, **71**, 909-922.
- Bäcklund, J. (1978), "On isoparametric elements", *Int. J. Num. Meth. Eng.*, **12**, 731-732.
- Gifford, L.N. (1979), "More on distorted isoparametric elements", *Int. J. Num. Meth. Eng.*, **14**, 290-291.
- Kikuchi, F., Okabe, M. and Fujio, H. (1999), "Modification of the 8-node serendipity element", *Comp. Meth. Appl. Mech. Eng.*, **179**, 91-109.
- Kohnke, P.C. (ed.), *ANSYS (1997) Theory Reference Release 5.4*, ANSYS, Inc., Canonsburg, PA.
- Lee, N.S. and Bathe, K.J. (1993), "Effects of element distortions on the performance of isoparametric elements", *Int. J. Num. Meth. Eng.*, **36**, 3553-3576.
- MacNeal, R.H. and Harder, R.L. (1992), "Eight nodes or nine?", *Int. J. Num. Meth. Eng.*, **33**, 1049-1058.
- MacNeal, R.H. (1994), *Finite Elements: Their Design and Performance*, Marcel Dekker: New York.
- Rajendran, S. and Liew, K.M. (2000), "Completeness requirements of shape functions for higher order finite elements", *Struct. Eng. Mech., An Int. J.*, **10**(2), 93-110.
- Rajendran, S. and Liew, K.M. (2003), "A novel unsymmetric 8-node plane element immune to mesh distortion under a quadratic displacement field", *Int. J. Num. Meth. Eng.*, **58**, 1718-1748.
- Stricklin, J.A., Ho, W.S., Richardson, E.Q. and Haisler, W.E. (1977), "On isoparametric vs. linear strain triangular elements", *Int. J. Num. Meth. Eng.*, **11**, 1041-1043.
- Timoshenko, S.P. and Goodier, J.N. (1934), *Theory of Elasticity*, 3rd Edn. McGraw-Hill Book Company: New York.
- Zienkiewicz, O.C. and Taylor, R.L. (1989), *The Finite Element Method Vol. 1: Basic Formulation and Linear Problems*, 4th Edn., McGraw-Hill Book Company, London.